Some Insights into Drop Impacts on a Hydrophobic Surface

A. Karn[1†], R. De[2] and A. Kumar[1]

[1]*Department of Mechanical Engineering, University of Petroleum and Energy Studies, Energy Acres, Bidholi, Dehradun, Uttarakhand, India 248007*
[2]*Department of Mechanical Engineering, University of Minnesota, Minneapolis, MN, 55414 USA*

†*Corresponding Author Email: akarn@ddn.upes.ac.in*

ABSTRACT

The current study reports the phenomenon of drop impacts on a hydrophobic surface in the substrate deposition regime (non-splashing), focusing on the characterization of each stage upon impact and different non-dimensional parameters involved such as spreading factor, recoil height and the durations of several phases. The results indicate that the drop dynamics is determined by an interplay of drop inertia, viscosity and surface tension. Apart from Reynolds number (*Re*) and Weber number (*We*) which are conventionally used to characterize drop impacts, a new non-dimensional impact parameter, $\xi \,(= We^{1/4}Re^{1/5})$ is introduced, and it is found out that the spreading factor and the different non-dimensional phase durations involved in the drop impact dynamics on a hydrophobic surface, scale fairly well with this newly defined impact parameter. Further, systematic studies into the non-dimensional durations of each phase upon impact, spreading factor and recoil factor (i.e. non-dimensional recoil height) with respect to different non-dimensional parameters are reported.

Keywords: Drop impact; Maximum drop spreading; Drop recoil; Impact parameter; Weber number.

NOMENCLATURE

D_0	pre-impact drop diameter		spreading in the second phase
D_{max}	maximum drop diameter upon impact	*We*	Weber number
H_{max}	maximum recoil height of drop after impact		
$M_1 - M_4$	four variants of glycerine-water mixture as defined in Table 1	τ_1	non-dimensional representation of t_{s1} ($= D_0/U_0\, t_{s1}$)
Re	Reynolds number	τ_2	non-dimensional representation of t_{r1} ($= D_0/U_0\, t_{r1}$)
U_0	pre-impact drop velocity		
t_{s1}	time taken between impact and maximum spreading in the first phase.	τ_3	non-dimensional representation of t_{s2} ($= D_0/U_0\, t_{s2}$)
t_{r1}	time taken between maximum spreading in the first phase and maximum recoil height in the first phase.	τ_4	non-dimensional representation of t_{r2} ($= D_0/U_0\, t_{r2}$)
t_{r2}	time taken between maximum spreading in the second phase and maximum recoil height in the second phase	β	spreading factor (non-dimensional spreading distance)
		α	recoil factor (non-dimensional recoil height)
t_{s2}	time taken between maximum recoil height in the first phase and maximum	ξ	impact parameter

1. INTRODUCTION

Drop impacts on liquid and solid surfaces have been widely studied for reasons that are relevant both in nature and in industry (Pasandideh-Fard *et al.*, 1996; Lastakowski *et al.*, 2014; Shen *et al.*, 2015; Kang, 2016; Soltani-Kordshuli and Eslamian, 2017). In nature, drop impacts are relevant for soil erosion, dispersal of microorganisms and spores and underwater noise during rainfall. Further, aeration of

surface layers of water bodies are related crucially to the air bubble entrapment due to rain drop impacts. Industrial relevance pertains to the wall/spray interactions in coating, spray cooling (Fedorchenko *et al.,* 2005), combustion and cleaning applications. Other technical applications of drop impacts include ink-jet printing (Minemawari *et al.,* 2011; Ersoy and Eslamian, 2019), rapid spray cooling of hot surfaces (turbine blades, rolls in rolling mills for steel production etc.), annealing, quenching of metals, fire suppression by sprinklers, internal combustion engines, solder bumps on printed circuit boards, and electric circuits in microelectronics produced by precision solder-drop deposition (Fedorchenko *et al.,* 2005).

The variation of the maximum diameter of the drop upon impact on a solid surface with the experimental parameters is a parameter of particular interest, for applications such as forensics and ink-jet printing, and that has been debated a lot in the existing literature (Laan *et al.,* 2014). Two main non-dimensional parameters usually employed to characterize the drop impact processes are Reynolds number ($Re = \rho D_0 U_0/\mu$) and Weber number ($We = \rho D_0 U_0^2/\sigma$) where D_0, U_0, ρ, σ, μ, and are the pre-impact diameter, pre-impact drop velocity, drop density, surface tension of the drop and the dynamic viscosity of the drop, respectively (Kumar *et al.,* 2017). There have been a large number of different models proposed in the literature for maximum spreading diameter, and sometimes different conclusions have been derived (Clanet, 2004; Roisman, 2009). Based on theory, when the spreading of a droplet is solely governed viscous forces, the non-dimensional spreading radius (or spreading factor) varies as $Re^{1/5}$ for $Re > 100$, although sometimes impact-spreading models also report a $Re^{1/4}$ scaling, particularly for the forensic applications (Laan *et al.,* 2014). On the other hand, for the capillary regime, there is another contention regarding two disparate scaling laws. Based on energy conservation, if there is a complete conversion of the kinetic energy into surface energy, the spreading factor scales as $We^{1/2}$ for $We > 100$. On the other hand, there is another perspective that takes both momentum and mass conservation into consideration and predicts a $We^{1/4}$ scaling. Thus, there lies a great necessity to substantiate the dependence of the spreading factor upon other experimental parameters. Further, to the authors' best knowledge, there is hardly any reported study that discusses the non-dimensional recoil heights of droplet upon impact.

Moreover, although a plethora of research has been reported on the different aspects of drop impacts on a solid surface (such as Chandra and Avedisian, 1991; Yarin and Weiss, 1995; Ukiwe and Kwok, 2005; Vadillo *et al.,* 2009; Wang and Chen, 2015, Roisman *et al.*, 2008, Kim and Rothstein, 2016, Boscariol *et al.*, 2018,Mostaghimi and Chandra, 2018, Brian *et al.,* 2019), systematic studies into the durations of each phase upon impact with respect to different liquid properties and across a wide range of non-dimensional numbers are also difficult to find. In particular, a recent study has investigated the flows inside a drop

upon impact with a solid surface and reported that the internal recirculation that develops inside an impacting a drop may have an important role in determining its subsequent dynamics including the pinch-off process (Kumar *et al.,* 2017). However, owing to the challenges involved in experimentally quantifying such flows, particularly the effect of drop curvature, it would be profitable to carry out simulations to study such flows. In order to ensure that the simulations accurately capture the physics of the phenomenon, it is required to validate the observable parameters such as the spreading distance, recoil height and the phase durations of different impact stages. Thus, an in-depth characterization of drop impacts across a wide range of non-dimensional parameters can also prove useful in the validation of computational results of drop impacts on a hydrophobic solid surface. Thus, in the current paper, we report the experimental results of the phenomenon of drop impacts in the substrate deposition regime (non-splashing), focusing on the characterization of each stage upon impact and its variation of different non-dimensional parameters. Such an understanding and characterizing of the various physical phenomena of drop impacts may also prove helpful in formulating reliable boundary conditions in numerical codes for spray simulation.

2. EXPERIMENTAL SETUP AND METHODOLOGY

2.1. Experimental Setup

The experiment is carried out to visualize and quantify the phenomenon of drop impacts on a solid surface. The experimental setup is shown in Fig. 1: It consists of a drop injection mechanism, an impact surface, an illumination source, a high speed camera for imaging and a data acquisition system. The drop injection mechanism includes a syringe to which needles of varying diameters could be attached. The syringe is mounted on a rigid frame, which ensures that all impacts of drops on the surface are orthogonal. The drops are produced using a mixture of water and Glycerine and the different conditions at which experiments were conducted are listed in Table 1 below. Mixture of water and glycerine is prepared with varying proportions to generate drops of different physical properties (i.e. diameter, and viscosity, etc.) and different pre-impact velocities – thus spanning a wide range of non-dimensional parameters *Re* and *We*. A Teflon-coated solid surface is used as a hydrophobic impact surface. A thin layer of silicone oil ($\nu = 10^{-5}\,m^2/s$, $\rho = 930\,kg/m^3$) is applied on the Teflon surface to ensure that surface imperfections can be ignored and the impact surface can be assumed as perfectly flat. Care is taken to ensure that before carrying out each experiment, the impact surface is freshly prepared. A Photonics high-speed Q-switch Nd:YLF laser is used as the illumination source in our experiments. The illumination source uses a maximum intensity of 30 mJ/pulse at 1 kHz at a peak wavelength of 527 nm and a pulse width of 150 ns. Further, the thickness of the pulsed light sheet is 500 μm and it operates at a repetition rate of
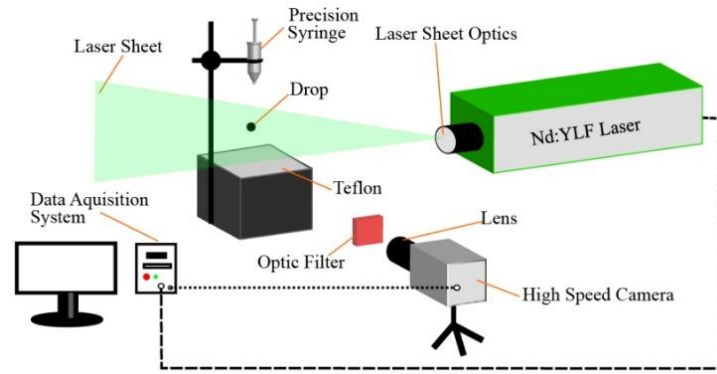
Fig. 1. Schematic of the experimental Setup.

Table 1 The range of variation of different parameters for the four liquids used in the experiments. The experiments are carried out at 21° C and ambient pressure of 101 kPa. Adapted from Kumar *et al.* (2017)

	Glycerin/ Water (v/v %)	Release Height (cm)	$\mu \times 10^3$ (kg/ms)	ρ (kg/m^3)	σ (kg/s^2)	We	Re / 10^3
M1	0/100	3.3 – 11.7	1.00	998.2	0.073	22-190	0.4-9.5
M2	10/90	5.1 – 16.5	1.31	1023.7	0.071	37-247	2.8-7.5
M3	30/70	2.5 – 21.1	2.50	1073.9	0.067	87-543	2.5-5.6
M4	50/50	7.9 – 18.0	5.00	1127.1	0.066	73-263	0.9-1.7

3000 frames per second. The light sheet is generated by a series of spherical and cylindrical lenses and it illuminates the symmetry plane of the drop. A Photron APX-RS camera captures the fluorescent particle images, operating at 3000 frames/ sec acquisition rate with a 1k × 1k pixel sensor. In order to minimize the ambient light, the reflections from the light source (λ = 527 nm) as well as to accentuate the signals from the fluorescent particles, a high pass optic filter is employed, that has a cut-off wavelength of 590 nm. To record the entire region of the drop dynamics, a micro Nikkor lens, 105 mm f/2.8 is employed. The magnification is unity, yielding a square field of view of 17.4 mm edge length, with a spatial resolution of 17 μm/pixel.

To determine the pre-impact drop diameter, measurements are made at several angular positions across the drop circumference. This process is repeated for four images prior to impact and finally a mean is computed. The drop velocity prior to impact is determined by the net displacement of the centroid of the drop. A cubic-spline interpolant is fitted on the velocity-time curve thus obtained and the pre-impact velocity is obtained at the instant of impact.

3. RESULTS AND DISCUSSION

3.1. Identification of the Different Processes in a Drop Impact

The outcome of the drop impact on the solid surface

depends upon the properties of the drop (surface tension, viscosity, compressibility), of the impacted surface, the fluid which the drop traverse through before impact, the impact velocity and the geometric aspects. In the case of drop impact on a solid surface, the main results can be spreading, bouncing or splashing (Yarin, 2006). The current paper deals with the phenomenon of drop spreading over a solid surface where the impact process generally involves four stages as shown in Fig. 2.: pre-impact (2a), spreading (2c), recoil (2e), and decay (2i). Usually, the spreading and recoil stages consist of multiple phases. As shown in Fig. 2, the pre-impact phase ranges from the point of drop ejection from the syringe till the impact. It is worth pointing out here that for all the liquid mixtures, the droplets possesses a non-zero velocity in the vertically downward direction after the second maximum recoil height is attained, and as the process of dissipative decay begins.

Upon impact, there is the outward radial spreading of the drop, leading to a very thin flattened disk shape which momentarily coming to rest. Then, after the spreading, the recoil of the drop occurs, with the drop moving inwards and upwards. The drop then attains a maximum height and then recoils back downwards. This sort of oscillation gives way to a dissipative decay process.

The high speed video was converted into individual frames and analysed for the drop morphology using image analysis in MATLAB. Figure 3 shows how the drop morphology changes with time, and goes through four different stages. For all these stages, a
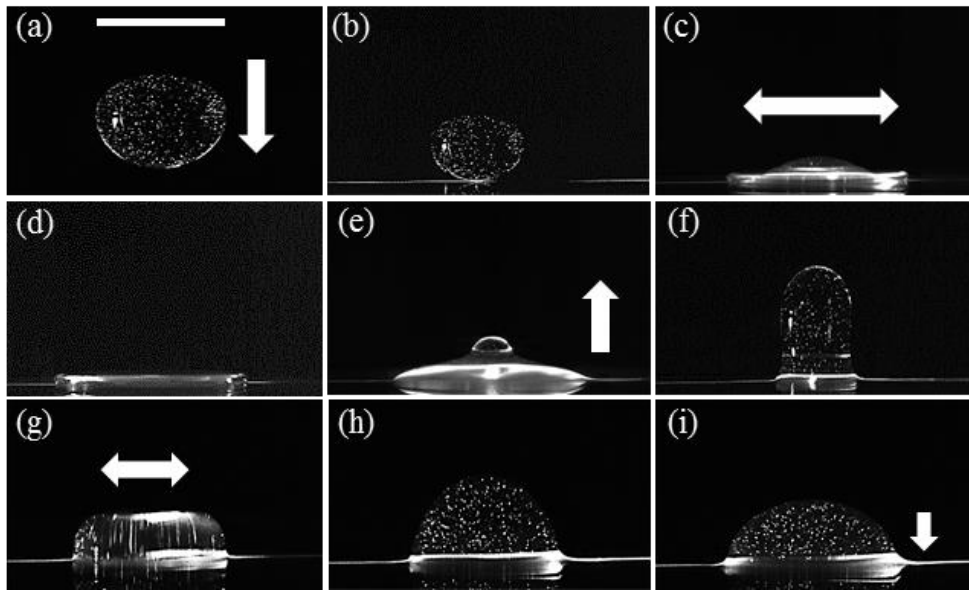
Fig. 2. Various stages in drop impact of an M2 droplet such as (a) Pre-impact, (b) Impact ($t = 0$), (c) Spreading, (d) Maximum spread ($t = t_{s1} \approx 25\ ms$), (e) Recoil, (f) Maximum Recoil height ($t = t_{r1} \approx 44\ ms$), (g) Maximum spread in the second phase ($t = t_{s2} \approx 66\ ms$) (h) Maximum Recoil height in the second phase ($t = t_{r2} \approx 85\ ms$) and (i) Subsequent phases and decay. The scale bar corresponds to a length of 4.5 mm.
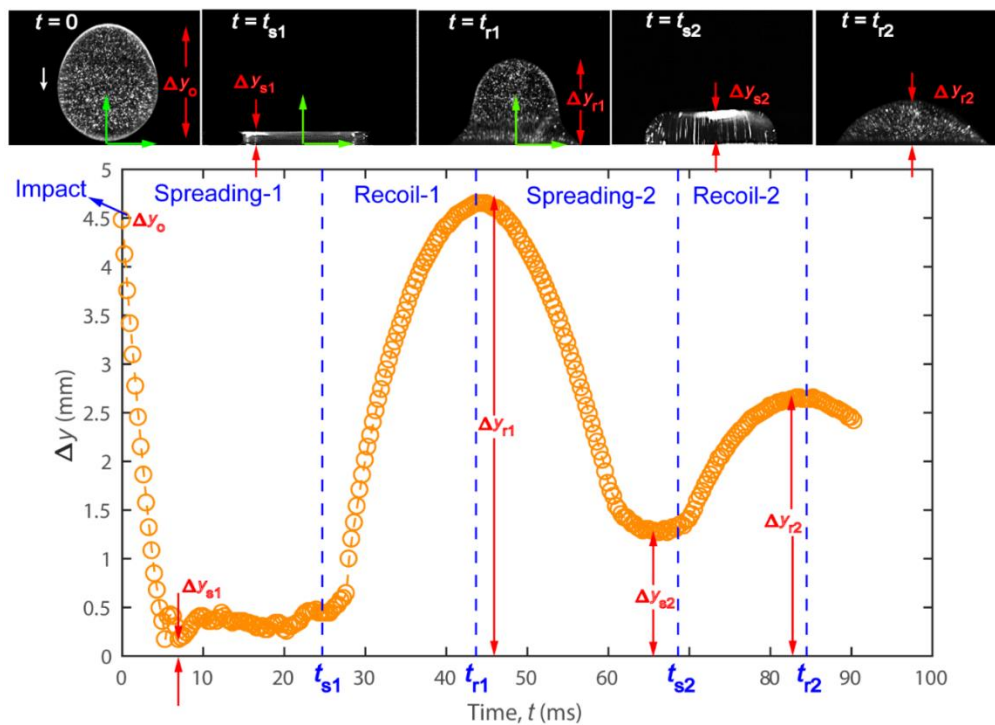
Fig. 3. The variation of Δy with respect to time for an M2 droplet released from a height of 91.4 mm. The origin is located on the impact surface such that the droplet centerline coincides with the origin. Figures above the plot are not to scale.

quantity Δy is defined as the distance between the topmost point on the droplet with respect to the origin, which is fixed on the impact surface coincident with the drop centreline. As evident from the figure, at the moment of drop impact ($t = 0$), Δy_o simply equals the droplet size and is

equivalent to D_o, i.e. 4.5 mm. The drop impact is followed by the first spreading phase. The droplet expands on the hydrophobic surface like a thin disk, and reaches its maximum diameter at $t \approx 25\ ms$ (t_{s1}), followed by the first recoil phase which terminates at $t \approx 44\ ms$ (t_{r1}). Δy at the

moment of maximum spreading in the first phase is termed as residual thickness and its value has been measured for the shown data as 0.16 mm, which is close to the prediction given in the prior literature as $\Delta y_{s1} = D_o Re^{-2/5}$, that yields a corresponding value of 0.15 mm (Josserand and Thoroddsen, 2016). The maximum height attained in the first recoil phase is denoted by Δy_{r1} and equals 4.8 mm. Then, the second spreading phase begins and lasts for a similar duration as the first spreading phase, ending at $t \approx 69\ ms\ (t_{s2})$, although the Δy_{s2} is considerably greater than its corresponding value in the first spreading phase. Next, a second recoil phase is observed with a significantly reduced recoil height till $t \approx 85\ ms\ (t_{r2})$. The second recoil phase is succeeded by significantly fast decay and dissipative processes.

Ihe maximum horizontal spread (D_{max}) and the maximum recoil height of the drop (Δy_{r1}), occurring in the first phase, are scaled with respect to drop diameter D_o and are represented as spreading factor, $\beta\ (= D_{max}/D_o)$ and recoil factor, $\alpha\ (= \Delta y_{r1}/D_o)$, respectively. For the second phase, these parameters are denoted by β_2 and α_2, and beginning from the drop impact, the time taken till the conclusion of the first spreading phase, first recoil phase, second spreading and second recoil phase are denoted by t_{s1}, t_{r1}, t_{s2} and t_{r2}, respectively. These variables are scaled with respect to D_0/U_0 and the corresponding non-dimensional parameters are expressed as $\tau_{s1}, \tau_{r1}, \tau_{s2}$ and τ_{r2}, respectively.

3.2. Different Regimes Produced Upon Drop Impact

Figure 4 shows different regimes upon drop impact. As the figure shows, at very low We, an 'elastic regime' exists, whereas at large values of Re and We, there is the occurrence of 'splash regime'.
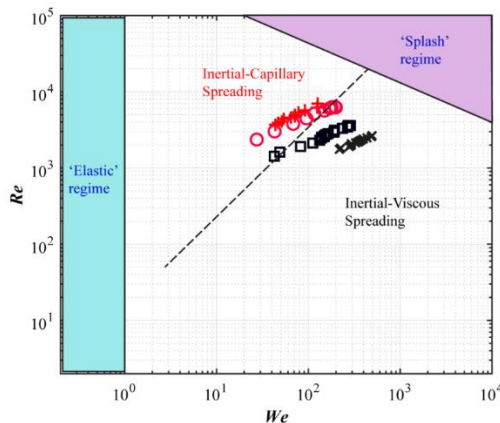
Fig. 4. The drop impact data of the current study overlaid on the plot showing different regimes of drop impact as a function of *We* and *Re* (adapted from Lagubeau *et al.,* 2012). Different markers correspond to liquid mixtures M1-M4.

The occurrence of splash is typically expected as the impact velocity increases, and is predicted by a classical splashing parameter, $K = We\sqrt{Re}$ that

was proposed by Mundo *et al.* (1995), incorporating the inertia, surface tension and viscous stresses. A lot of effort has gone into finding the critical values of K for various impact conditions, although a splash is expected for $K \geq 3000$ (Josserand and Thoroddsen, 2016). However, in our experiments no splash is observed in the range of 927 – 25462, which leads to the conclusion that the thin silicone oil coating on the Teflon surface may have a significant role to play in the drop impact dynamics. Cossali *et al.* (1997), based on the experimental data of Mundo *et al.* (1995) and others, correlated the minimum value of the K number for splashing (Ks) with a constant on account of droplet inertia, as well as the dimensionless roughness amplitude with respect to droplet diameter R_{nd} as, $K = We\ Oh^{-0.4} = 649 + 3.76\ /\ R_{nd}^{0.63}$. Further, another drop splash criterion has been suggested by Yarin and Weiss (1955) in terms of the experimental threshold velocity for drop splashing as $V_{th} = 18\ (\sigma/\rho)^{1/4}\ (\mu/\rho)^{1/8}\ f^{3/8}$, where f can be replaced with V/D for a single impact on a pre-existing liquid film (Yarin, 2006). The calculations for all the cases of drop impacts in our experiments indicate that the impact velocity of drops is considerably lower than the threshold velocity required for drop splashing. Thus, it is observed that the drop spreads over the wall like a lamellae with a visible outer rim. In the absence of splashing, the liquid simply spreads on the surface, and then recedes or remain close to this maximum spread, for instance when the liquid viscosity is very high (Rioboo *et al.,* 2001). In fact, the dynamics of the drop upon impact is determined by a subtle balance between inertia, viscous and capillary forces (Bartolo *et al.,* 2005). Thus, depending upon whether viscous forces or capillary forces dominate, the spreading dynamics can be termed as 'Inertial-viscous spreading' or 'Inertial-capillary spreading'. In the inertial-viscous regime, the kinetic energy of the drop is mostly lost to viscous dissipation, whereas when the fluid viscosity can be neglected, the balance exists between inertia and surface-tension (Eggers *et al.,* 2010)

3.3. Non-Dimensional Spreading Diameter of the Impacted Drop

Figure 5 presents the variation of β with respect to *We* and *Re* for the four different liquid mixtures. As the Fig. 5(a) shows, β increases with an increase in *We* for all the mixtures. When the drop strikes the surface with some velocity, spreading is largely influenced by the kinetic energy of the drop, although the surface energy is also important. Both the surface and the kinetic energy of the drop are dissipated by viscous forces in the thin expanding liquid disk, and since the liquid disk is expanding, it gets converted into surface energy. Under the inertia-dominated impact of drops such as in our experiments, the rapidly moving liquid on the upper part of the formed neck, impinges on the slowly moving liquid below, thus pushing the oncoming liquid radially outward. In this inertial-viscous regime the maximum drop deformation is given by a balance between kinetic energy and viscous dissipation, and β is given as $\beta - 1 \propto Re^{1/5}$, or

simply $\beta \propto Re^{1/5}$, as suggested by Rein (1993), and more recently by Rosiman (2009). The underlying principles behind this expression are volume conservation and energy conservation. The volume conservation entails: $\pi D_{max}^2 h = \pi D_0^3/6$, thus giving an expression for the height of the liquid disk at the point of maximum expansion as $h = D_0^3/6D_{max}^2$. Similarly, the initial pre-impact kinetic energy of the drop is given as $\pi D_0^3 \rho U_0^2/12$, and the energy dissipation by viscous forces has been estimated as $\mu U_0 D_{max}^3/h$ (Clanet, 2004). Substituting for the height of the liquid disk as obtained from the volume conservation, the energy dissipation can be expressed as $6\rho U_0^2 D_0^3 \beta^5/Re$.

(a)

(b)
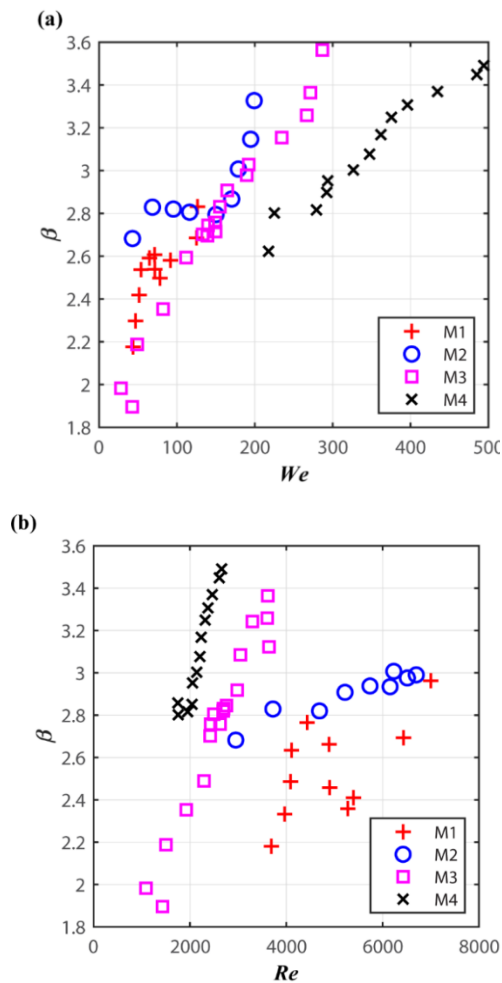
Fig. 5. Non-dimensional spreading distance (β) and its variation with respect to (a) *We*, and (b) *Re*. Different markers correspond to liquid mixtures M1-M4.

In the limiting case, the initial kinetic energy should equal the viscous dissipation, thus giving as expression of the form $\beta \propto Re^{1/5}$. Such an expression would be particularly valid for liquids of high viscosity as pointed out by Roisman (2009). In the inertial- capillary regime of drop spreading, the spreading factor is given by a more intricate balance between inertia and capillary forces, with some correction due to viscous dissipation and wettability

effects. For instance, a simple scaling analysis comparing the initial kinetic energy of the drop at impact with surface energy at the maximum spreading radius suggests an expression of the type $\beta \propto We^{1/4}$ (Josserand and Thoroddsen, 2016). Based on the calculations of velocity and acceleration of the impacting drop along with volume conservation, Clanet *et al.* (2004) deduced that β should scale as $We^{1/4}$. According to Clanet (2004), this law should hold good, particularly for liquids of low viscosity. Figure 6(a) presents specifically the prediction of β with respect to *We* according to Clanet (2004) and its comparison for the mixture M1 which has a low viscosity. Similarly, Fig. 6(b) illustrates the prediction of β with respect to *Re* according to Roisman (2009) and its comparison for the high viscosity mixture M4. As is fairly evident from these plots, the expression of Clanet (2004) and Roisman (2009) indeed predict the spreading factor β quite closely, for mixtures of low and high viscosity, respectively.

(a)

(b)
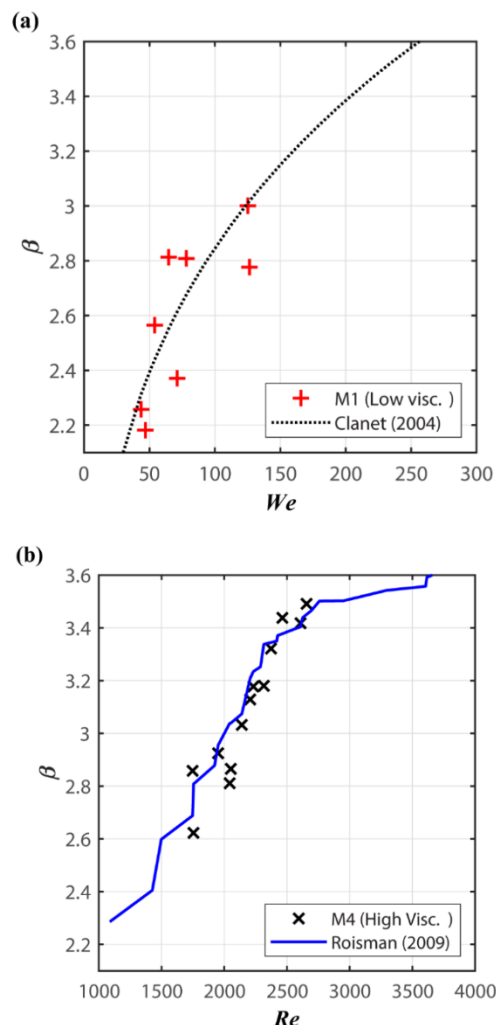
Fig. 6. Variation of Non-dimensional spreading distance (β) with respect to (a) *We* along with the nearness of fit with the predictions of Clanet (2004) for a low viscosity fluid, and (b) *Re* along with the close fit of the data with the expression of Roisman (2009) for a high viscosity fluid.

However, the dynamics of drop spreading are governed, not only between inertia and viscosity but a subtle balance between these forces along with capillary forces (Bartolo *et al.,* 2005). Hence, to assess the cumulative effects of inertia, surface tension and viscosity, a non-dimensional impact parameter is defined as $\xi = We^{1/4}Re^{1/5}$. Interestingly, the plot of β vs. ξ shows an insightful trend, as presented in Fig. 7 below. As Fig. 7 shows, all the data points converge on a straight line, suggesting that ξ may be a relevant parameter that captures the competing physical effects that determine drop spreading. Using linear regression, the slope and intercept of the straight line are 0.134 and 0.539, respectively. In conclusion, the drop spreading is a phenomenon that is limited both by capillarity, as well as by viscosity depending upon the liquid and the surface properties.
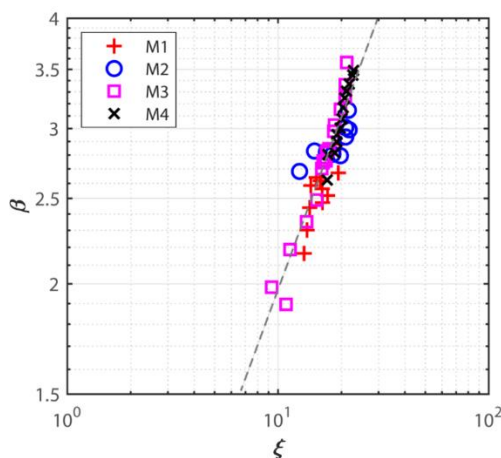

Fig. 7. Variation of β with respect to ξ for different liquid mixtures. The regression line has a slope and intercept of 0.134 and 0.539, respectively.

3.4. Non-Dimensional Recoil Height

Among the four liquids/ liquid mixtures, liquid M1 shows jetting and breakup of a tiny drop for M1, and makes the measurement of non-dimensional recoil height inaccurate. On the other hand, for the liquid mixture M4, viscous dissipation is so large that no significant drop recoil is observed. Figure 8 illustrates the relationship between α and We for two liquid mixtures M2 and M3. An important observation from the plotted data is that α increases slightly with increase in We. For M2 mixture, α increased from 1 to 1.2, as We underwent a fourfold increment from 50 to 200. For M3 mixture, α increased from 0.82 to 0.97 as We varied between 50 – 290. Using linear regression, the slopes for the fitted linear-curve have been determined as 0.0007 and 0.0004 and the intercepts are 0.9253 and 0.8161 for M2 and M3, respectively. For a particular liquid mixture, an increase in We implies an increasing dominance of inertial effects over surface tension. A greater dominance of inertial effects favors a greater drop recoil and overcomes the effect of surface tension that impedes greater drop deformation, as the drop recoils back from its maximum spreading. Thus, an increase in drop recoil height is observed with respect to an increment in We. In general, at a given We, α values are greater for M2 as compared to M3 because of the difference in viscosity of the mixtures. Since M3 has a greater viscosity, a greater amount of viscous dissipation is observed during the contraction phase. A limiting case of this viscous dissipation is observed for the highly viscous liquid M4, where there is negligible kinetic (or inertial) energy left with the drop, as it starts to rise from the horizontal surface.
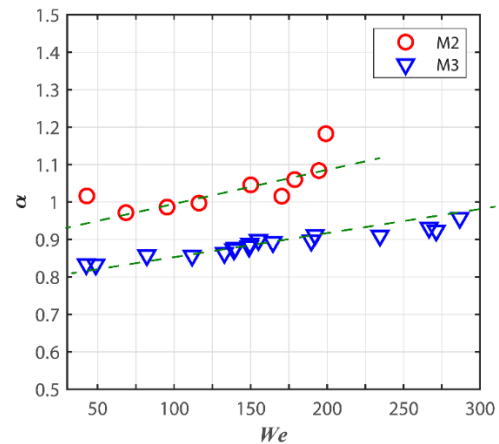

Fig. 8. Variation of non-dimensional recoil height (α) with respect to We for two liquid mixtures of intermediate viscosity. For M2 and M3, the slopes of the regression line are 0.0007 and 0.0004, and the intercepts are 0.9253 and 0.8161, respectively.

3.5 Non-Dimensional Phase Durations

Finally, we focus our attention on the non-dimensional phase durations for the different processes in drop impact. Beginning from the drop impact, the time taken till the conclusion of the first spreading phase, first recoil phase, second spreading and second recoil phase are denoted by t_{s1}, t_{r1}, t_{s2} and t_{r2}, respectively. These variables are scaled with respect to D_0/U_0 and the corresponding non-dimensional parameters are expressed as $\tau_{s1}, \tau_{r1}, \tau_{s2}$ and τ_{r2}, respectively.

Figure 9 illustrates the variation in the non-dimensional phase durations of the first expansion, first contraction, second expansion and second recoil phase, respectively with respect to the impact parameter. It is clear from all the four plots that τ_1, τ_2, τ_3 and τ_4 scale pretty well with ξ, as the data for all the liquids converge on the same linear curve. The slopes of the linear curves have been determined from linear regression to be 0.1728, 0.5469, 0.3915 and 0.2968 for the four non-dimensional phase durations, respectively. Similarly, the four intercepts are -1.1109, -2.0520, -2.0760 and -1.3328, respectively for the four phase durations, as obtained from linear regression. As the figure demonstrates, an increase in impact parameter invariably leads to an increase in τ_1. This is evident since an increase in impact parameter
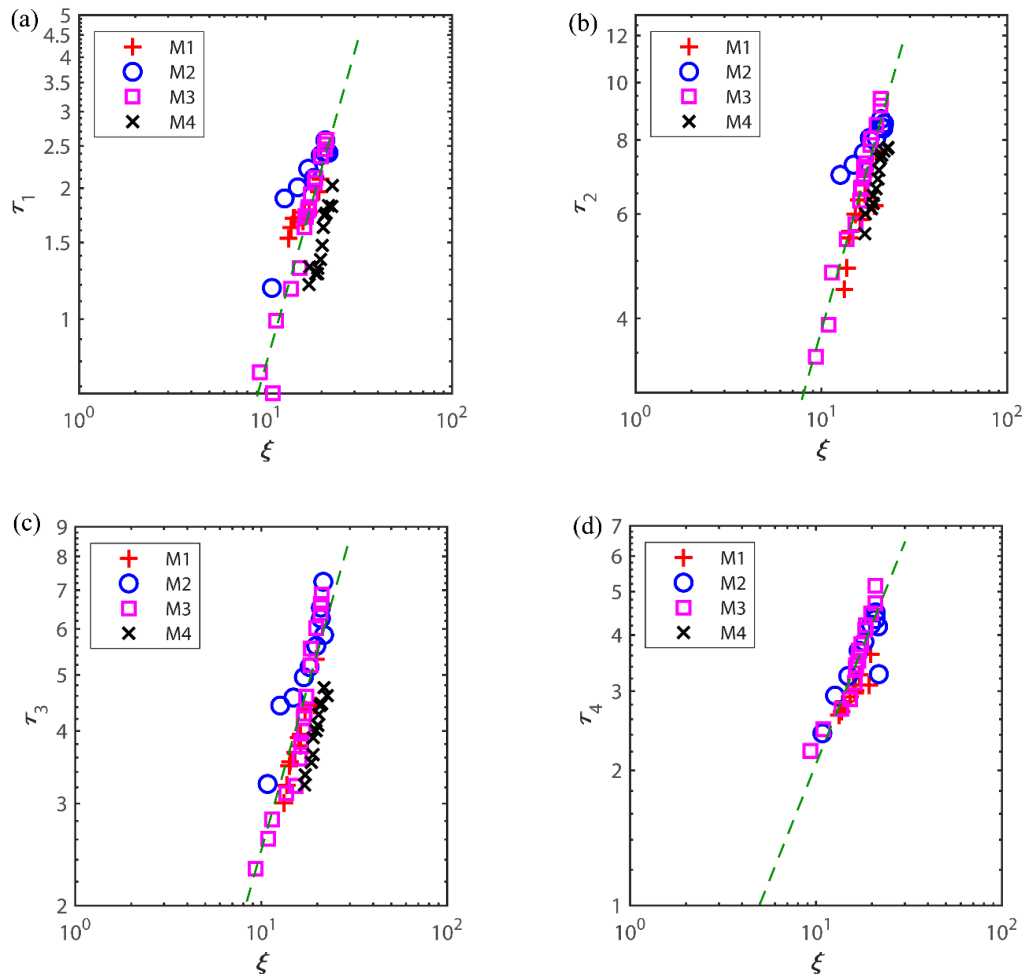
Fig. 9. Variation of (a)τ_1 (Slope: 0.1728, Intercept: −1.1109),
(b) τ_2 (Slope: 0.5469, Intercept: −2.0520), (c) τ_3 (Slope: 0.3915, Intercept: −2.0760), and
(d)τ_4 (Slope: 0.2968, Intercept: −1.3328) , with respect to non-dimensional parameter ξ.

invariably signifies a rise in inertial effects, which leads to greater drop spreading spanning over a larger time scale. Further, a comparison of τ_1 and τ_3 shows that between the first phase and the second phase, τ_3 is somewhat larger than τ_1. This is because of the sluggish response of drop in the second phase, i.e. with decreased kinetic energy, it takes longer for the drop to attain maximum spreading in the second phase. However, during the recoil phase, the trend is found to be opposite, although for a different reason. As the figure shows, τ_2 is somewhat larger than τ_4. This is only because of the fact that on account of the reduced kinetic energy, the upward recoil in the second phase is fairly minimal and is attained quickly. In addition, for highly viscous liquids, it might take a much longer time to attain the maximum recoil height in the second phase (and thus not shown in the figure).

4. CONCLUSION

To sum it up, in the present work, drop impact on a solid surface under the spreading regime has been explored for four different liquids/ liquid mixtures.

The parameters of interest were non-dimensional spreading distance, non-dimensional drop recoil height and the phase durations of different processes that occur after impact. Depending upon whether viscous forces or capillary forces dominate, the spreading dynamics of drops can be termed as 'inertial-viscous regime' or 'inertial capillary regime'. The non-dimensional spreading factor, β increases with increase in *We* or *Re* for all the mixtures. In the inertial-viscous regime of drop impact, which is closely observed in liquids of high viscosity, i.e. M4, β scales as $\beta \propto Re^{1/5}$, similar to the reports of Rein (1993) and Roisman (2009). On the other hand, in the inertial-capillary regime, which is closely observed in liquids of low viscosity M1, β scales as $\beta \propto We^{1/4}$. Further, a new non-dimensional impact parameter was defined as $\xi = We^{1/4}Re^{1/5}$, such that all the β vs. ξ data converge on the same line for all the liquid mixtures, suggesting that ξ captures the competing effects of inertia, viscosity and surface tension that are relevant in the drop spreading upon impact. Similarly, all the non-dimensional phase durations, τ_1, τ_2, τ_3 and τ_4 are found to scale pretty well with ξ.

REFERENCES

Bartolo, D., C. Josserand and D. Bonn (2005). Retraction dynamics of aqueous drops upon impact on non-wetting surfaces. *Journal of Fluid Mechanics 545*, 329-338.

Boscariol, C., S. Chandra, D. Sarker, C. Crua and M. Marengo (2018). Drop impact onto attached metallic meshes: liquid penetration and spreading. *Experiments in Fluids* 59(12), 189.

Brian, D., Ahmadian-Yazdi, M. R., Barratt, C., & Eslamian, M. (2019). Impact dynamics and deposition of perovskite droplets on PEDOT: PSS and TiO2 coated glass substrates. *Experimental Thermal and Fluid Science*, 105, 181-190.

Chandra, S. and C. T. Avedisian (1991). On the collision of a droplet with a solid surface. *Proceedings of the Royal Society of London. Series A: Mathematical and Physical Sciences* 432(1884), 13-41.

Clanet, C., C. Béguin, D. Richard and D. Quéré (2004). Maximal deformation of an impacting drop. *Journal of Fluid Mechanics 517*, 199-208.

Cossali, G. E., A. Coghe and M. Marengo (1997). The impact of a single drop on a wetted solid surface. *Experiments in Fluids* 22, 463–72.

Eggers, J., M. A. Fontelos, C. Josserand and S. Zaleski (2010). Drop dynamics after impact on a solid wall: theory and simulations. *Physics of Fluids* 22(6), 062101-062109.

Ersoy, N. E. and M. Eslamian (2019). Capillary surface wave formation and mixing of miscible liquids during droplet impact onto a liquid film. *Physics of Fluids* 31(1), 012107.

Fedorchenko, A. I., A. B. Wang and Y. H. Wang (2005). Effect of capillary and viscous forces on spreading of a liquid drop impinging on a solid surface. *Physics of Fluids* 17(9), 093104-093111.

Josserand, C. and S. T. Thoroddsen (2016). Drop impact on a solid surface. *Annual review of fluid mechanics* 48, 365-391.

Kang, B. (2016). Experimental study of the phenomenon of droplet impact upon a liquid surface. *Journal of Applied Fluid Mechanics 9*(2), 757-765.

Kim, J. H. and J. P. Rothstein (2016). Droplet impact dynamics on lubricant-infused super hydrophobic surfaces: The role of viscosity ratio. *Langmuir 32*(40), 10166-10176.

Kumar, S. S., A. Karn, R. E. Arndt and J. Hong (2017). Internal flow measurements of drop impacting a solid surface. *Experiments in Fluids 58*(12), 1-9.

Laan, N., K. G. de Bruin, D. Bartolo, C. Josserand and D. Bonn (2014). Maximum diameter of impacting liquid droplets. *Physical Review Applied* 2(4), 044018-044022.

Lagubeau, G., M. A. Fontelos, C. Josserand, A. Maurel, V. Pagneux and P. Petitjeans (2012). Spreading dynamics of drop impacts. *Journal of Fluid Mechanics* 713, 50-60.

Lastakowski, H., F. Boyer, A. L. Biance, C. Pirat and C. Ybert (2014). Bridging local to global dynamics of drop impact onto solid substrates. *Journal of Fluid Mechanics 747*, 103-118.

Minemawari, H., T. Yamada, H. Matsui, J. Y. Tsutsumi, S. Haas, R. Chiba, R. Kumai and T. Hasegawa (2011). Inkjet printing of single-crystal films. *Nature 475*(7356), 364-367.

Mostaghimi, J., and S. Chandra (2018). Droplet Impact and Solidification in Plasma Spraying. *Handbook of Thermal Science and Engineering*, 2967-3008.

Mundo, C. H. R., M. Sommerfeld and C. Tropea (1995). Droplet-wall collisions: experimental studies of the deformation and breakup process. *International journal of multiphase flow 21*(2), 151-173.

Pasandideh-Fard, M., Y. M. Qiao, S. Chandra and J. Mostaghimi (1996). Capillary effects during droplet impact on a solid surface. *Physics of Fluids* 8(3), 650-659.

Rein, M. (1993). Phenomena of liquid drop impact on solid and liquid surfaces. *Fluid Dynamics Research 12*(2), 61-93.

Rioboo, R., C. Tropea and M. Marengo (2001). Outcomes from a drop impact on solid surfaces. *Atomization and sprays* 11. 1-12.

Roisman, I. V., E. Berberović and C. Tropea (2009). Inertia dominated drop collisions. I. On the universal flow in the lamella. *Physics of fluids* 21(5), 052103-052111.

Roisman, I., L. Opfer, C. Tropea, M. Raessi, J. Mostaghimi and S. Chandra (2008). Drop impact onto a dry surface: Role of the dynamic contact angle. *Colloids and Surfaces A: Physicochemical and Engineering Aspects* 322(1-3), 183-191.

Shen, Y., J. Tao, H. Tao, S. Chen, L. Pan and T. Wang (2015). Relationship between wetting hysteresis and contact time of a bouncing droplet on hydrophobic surfaces. *ACS applied materials & interfaces* 7 (37), 20972-20978.

Soltani-Kordshuli, F. and M. Eslamian (2017). Impact dynamics and deposition of pristine and graphene-doped PEDOT: PSS polymeric droplets on stationary and vibrating substrates. *Experimental Thermal and Fluid Science* 89, 238-248.

Ukiwe, C., and D. Y. Kwok (2005). On the maximum spreading diameter of impacting droplets on well-prepared solid surfaces. *Langmuir* 21(2), 666-673.

Vadillo, D. C., A. Soucemarianadin, C. Delattre and D. C. Roux (2009). Dynamic contact angle effects onto the maximum drop impact spreading on solid surfaces. *Physics of Fluids* 21(12), 122002-122012.

Wang, Y. and S. Chen (2015). Droplets impact on textured surfaces: mesoscopic simulation of spreading dynamics. *Applied Surface Science* 327, 159-167.

Yarin, A. L. (2006). Drop impact dynamics: splashing, spreading, receding, bouncing.... *Annual Review of Fluid Mechanics 38*, 159-192.

Yarin, A. L. and D. A. Weiss (1995). Impact of drops on solid surfaces: self-similar capillary waves, and splashing as a new type of kinematic discontinuity. *Journal of Fluid Mechanics* 283, 141-73.